GEOLOGICA CARPATHICA, FEBRUARY 2014, 65, 1, 83–95 doi: 10.2478/geoca-2013-0006

Composition and alteration of Cr-spinels from Milia and Pefki serpentinized mantle peridotites (Pindos Ophiolite Complex, Greece)

ARGYRIOS KAPSIOTIS

Department of Geology, Section of Earth Materials, Panepistimiopolis of Rion, University of Patras, 265 04 Patras, Greece;
Present address: Department of Earth Sciences, Sun Yat-sen University, 510275 Guangzhou, P.R. China; kapsiotisa@yahoo.gr

(Manuscript received May 9, 2013; accepted in revised form October 16, 2013)

Abstract: The Pindos Ophiolite rocks include variably serpentinized peridotites derived from a harzburgitic and subordinately dunitic mantle. In the serpentinized matrix of these rocks pseudomorphic (mesh, bastite) and non-pseudomorphic (interpenetrating, type-2 hourglass) textures were recognized. Chromian spinel (Cr-spinel) is anhedral to subhedral and often replaced by a porous opaque phase. Chemistry data show that Cr-spinel cores retain their original composition, having Cr#[Cr/(Cr + Al)] that ranges between 0.45 and 0.73, and Mg#[Mg/(Mg + Fe^{2+})] that varies between 0.52 and 0.65, accompanied by low content in TiO_2 (< 0.11 wt. %). The relatively wide variation of their Cr# values reflects that the studied peridotites were produced by variable degrees of melting. It is likely that the Pindos peridotites represent mantle residues originally formed in a mid-ocean ridge (MOR) environment, which were subsequently entrapped as part of a mantle wedge above a supra-subduction zone (SSZ) regime. Cr-spinel adjacent to clinochlore systematically displays limited compositional and textural zoning along grain boundaries and fractures. However, the degree of peridotite serpentinization does not correlate with the abundance of zoning effects in accessory Cr-spinel. Thus, Cr-spinel zoning is thought to represent a secondary feature obtained during the metamorphic evolution of the host peridotites. Core to rim compositional trends are expressed by MgO and Al_2O_3 impoverishment, mainly compensated by Cr_2O_3 and FeO increases. Such chemical trends are produced as a result of Cr-spinel re-equilibration with the surrounding serpentine, and their subsequent replacement by ferrian (Fe^{3+}-rich) chromite and clinochlore, respectively, during a brief, fluid assisted, greenschist facies metamorphism episode (T > 300 °C). The limited occurrence of ferrian chromite with high Fe^{3+}# values suggests that elevated oxidizing conditions were prevalent only on a local scale during Cr-spinel alteration.

Key words: Pindos, metamorphism, peridotites, Cr-spinel, ferrian chromite.

Introduction

Chromian spinel [hereafter Cr-spinel, $(Mg,Fe^{2+})(Cr,Al,Fe^{3+})_2O_4$] is a common accessory mineral in ultramafic and mafic rocks. Its composition has often been used as a sensitive indicator in order to determine the degree of partial melting in the mantle source region and/or the composition of the produced mafic melt (e.g. Dick & Bullen 1984; Arai 1992; Zhou et al. 1998; Proenza et al. 1999; Barnes & Roeder 2001; Hellebrand et al. 2001; Kamenetsky et al. 2001; Zhou et al. 2005; González-Jiménez et al. 2011). In addition, variations concerning Cr-spinel composition in peridotites are also known to reflect dissimilarities in the processes involved in the evolution of upper mantle rocks, such as partial melting and mantle metasomatism (e.g. Kubo 2002; Arif & Jan 2006), or even discrepancies in the geotectonic setting in which they were formed (e.g. Ishii et al. 1992; Ahmed et al. 2012).

Compared to other high-T igneous phases Cr-spinel is thought to be resistant to post-magmatic processes such as alteration and regional metamorphism (e.g. Burkhard 1993; Barnes 2000; Mellini et al. 2005). Therefore, it is especially useful in evaluating the tectonic provenance of strongly hydrated mantle peridotites (serpentinites), since it commonly represents the only preserved primary phase (e.g. Saumur & Hattori 2013). However, there is now plenty of convincing evidence that Cr-spinel may undergo significant chemical modifications related to sub-solidus equilibration during the post-magmatic stage. More specifically, textural observations and mineral chemistry data indicate that hydrothermal alteration and metamorphism can significantly modify primary Cr-spinel composition (e.g. Bliss & MacLean 1975; Evans & Frost 1975; Wylie et al. 1987; Kimball 1990; Suita & Streider 1996; Barnes 2000; Mellini et al. 2005; Farahat 2008; Merlini et al. 2009; Rollinson et al. 2012; Sansone et al. 2012).

High Cr/Al, low Mg/Fe^{2+} and considerable to high Fe^{3+} contents describe the most common alteration trend of Cr-spinel. The composition of this alteration product can be expressed as $(Fe^{2+},Fe^{3+},Mg)(Cr,Fe^{3+},Fe^{2+},Al)_2O_4$ and is known in the literature as ferrian chromite (formerly called 'ferritchromite' or 'ferritchromit', Spangenberg 1943; and cited in, among others, Evans & Frost 1975; González-Jiménez et al. 2009; Mukherjee et al. 2010; Gervilla et al. 2012; Derbyshire et al. 2013). Various investigations suggest that ferrian chromite forms during low-T hydrothermal alteration (e.g. Burkhard 1993; Wylie et al. 1987; Mukherjee et al. 2010). However, the majority of studies indicate that ferrian chromite is produced as a consequence of metamorphism (e.g. Bliss & MacLean 1975; Barnes 2000; Proenza et al. 2004; Mellini et al. 2005; Merlini et al. 2009; Grieco & Merlini 2012).

The present paper discusses the compositional variability of accessory Cr-spinels from a set of mantle peridotite bodies, located in the areas of Milia and Pefki, Pindos Ophiolite Complex, Greece. In this study, Cr-spinel compositions are used as a petrogenetic tool to conclude the genesis and geotectonic origin of the studied mantle peridotites. Moreover, the current study attempts to provide insights into the influence of serpentinization and metamorphism on Cr-spinels, with the aim of explaining their alteration patterns on the basis of textural and mineral chemistry data.

Geological framework

The External Hellenides are part of the Alpine orogenic belt, representing a typical fold-thrust belt. They are mainly composed of Mesozoic and Cenozoic sedimentary rocks deposited in a series of platforms (pre-Apulian and Gavrovo Zones) and basins (Ionian and Pindos Zone). According to Jones & Robertson (1991) the Pindos Zone is made up of a series of Mesozoic and Tertiary tectono-stratigraphic units including: 1) the Pindos Ophiolites (Jurassic), 2) the shallow-water Orliakas limestones (Late Cretaceous), 3) the Avdella Mélange (Late Triassic–Late Jurassic), 4) the Dio Dendra Group deep-water sediments (Late Jurassic–Late Cretaceous) and 5) the Pindos flysch (Late Cretaceous–Tertiary).

The ophiolites of northwestern continental Greece are considered to be oceanic remnants after the progressive closure of the Neotethyan Ocean. Among these the Pindos Ophiolite Complex (Fig. 1) has been extensively studied with regard to its structural features and tectonic position (e.g. Ross & Zimmerman 1996; Rassios & Smith 2000; Rassios & Moores 2006; Ghikas et al. 2009; Rassios & Dilek 2009).

The Pindos Ophiolite Complex is located in northwestern Greece and corresponds to a piece of Middle to Upper Jurassic oceanic crust (Rassios & Smith 2000). It is tectonically emplaced over the autochthonous Maastrichtian-Eocene Pindos flysch. It can be subdivided into four principal tectonic units: the Dramala Ultramafic Complex, the Loumnitsa Unit and the Aspropotamos Complex, all structurally overlying a sub-ophiolitic chaotic lithological formation known as the Avdella Mélange (Jones & Robertson 1991). The Dramala Complex represents oceanic mantle and part of its crustal sequence and comprises variably depleted spinel harzburgite–dunite masses (>1000 km^2), which may host small chromitite pods, pyroxenite and ultramafic cumulates (Jones & Robertson 1991). Lo-

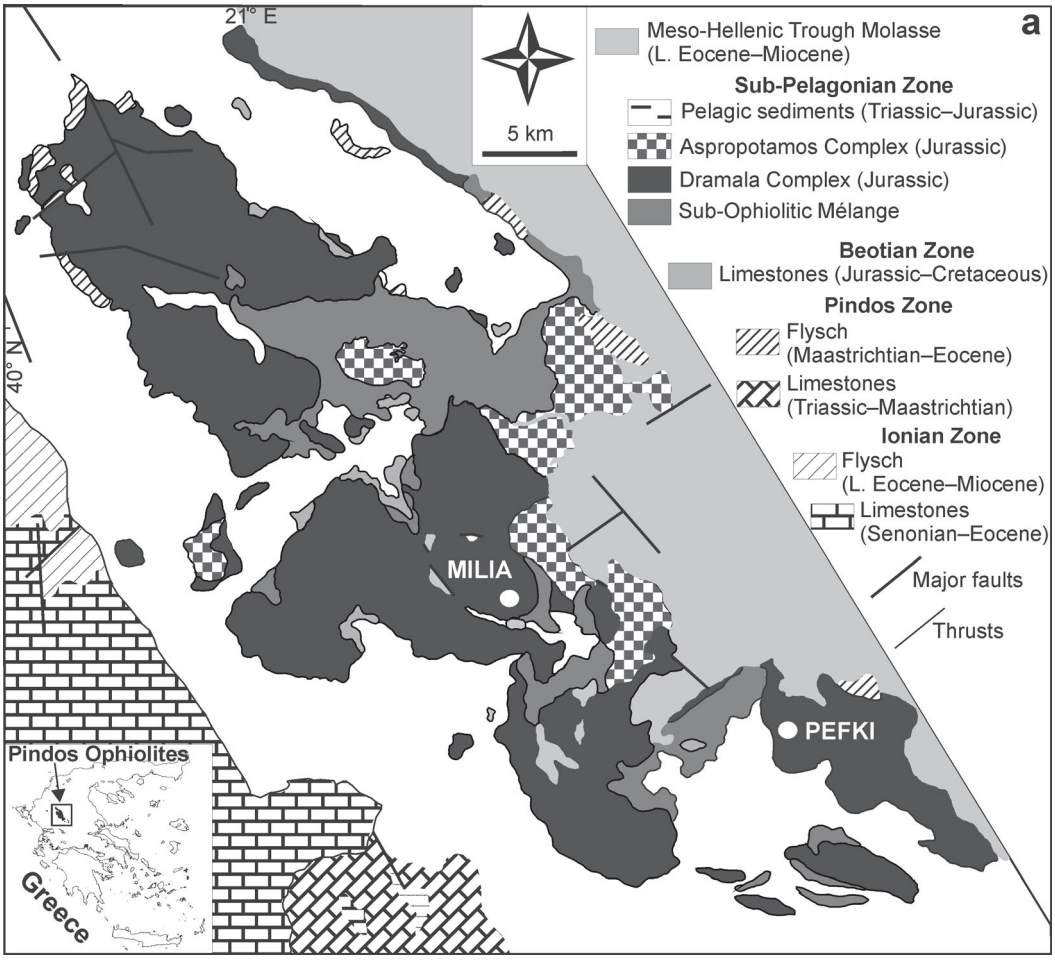

Fig. 1. Simplified geological map of the Pindos Ophiolite Complex showing the location of the areas of Milia and Pefki (modified after Jones & Robertson 1991) and inset map illustrating the location of the Pindos Ophiolites in the Greek peninsula.

cally, harzburgite and chert breccias are cemented by ophicalcite, indicating that the Dramala ultramafic rocks were once exposed on the sea floor (Jones et al. 1991). The intrusive and extrusive crustal rocks of the Aspropotamos Complex cover a wide range of geochemical affinities, varying from N-MORB through MORB/IAT to IAT and boninites cross-cutting all the previous types of volcanics (Kostopoulos 1989). The Loumnitsa Unit represents the metamorphic sole of both Dramala and Aspropotamos complexes, consisting of low amphibolite- and greenschist-facies metaigneous and metasedimentary rocks that have yielded amphibole Ar-Ar ages of 169 ± 5 and 165 ± 3 Ma (Whitechurch & Parrot 1978; Spray & Roddick 1980). The Avdella Mélange represents a subduction-accretion formation and includes sediments, volcanic and plutonic rocks, as well as metamorphic rocks of the Loumnitsa Unit.

Sampling and field observations

A total of 17 serpentinized peridotite samples were collected from the Pindos Ophiolite Complex. The peridotite samples were taken from the Milia and Pefki districts, each of them located in the southeastern part of the Dramala Massif. Care was taken to sample variably serpentinized rocks from different mantle lithologies.

The studied areas are extremely mountainous (with summits between 1500 and 2150 m above sea level). Extensive outcrops of peridotites are well exposed both in Milia and Pefki. The peridotites are coarse-grained and strongly deformed. Deformed massive and variably serpentinized harzburgite is the dominant rock type in the mantle section of both investigated regions, commonly cross-cut by pyroxenite dykes and gabbroic veins, especially in the area of Pefki. Milia harzburgites may contain blocky-shaped pyroxene, which probably represents a preserved high-T 'asthenospheric' (or 'mantle') fabric (Rassios & Dilek 2009). On the other hand, dunite is subordinate to harzburgite in both areas and relatively more uncommon in the area of Pefki. Dunite occurs in the form of small pods or bodies ranging from a few m to a few tens of m in size. The largest dunite bodies commonly host podiform chromitites. The contact between harzburgite and dunite is transitional and frequently sheared and serpentinized. Moreover, dunite is commonly more serpentinized and mylonitized compared to harzburgite.

Serpentinization is almost pervasive through the whole mantle section in Milia, whereas in Pefki serpentinization effects are only local within the ultramafic section. Serpentinized rocks are frequently strongly deformed, displaying foliation along sizeable shear zones (a few m in thickness), which further indicates that these rocks were affected by regional metamorphism. They are commonly covered by a thick reddish to dark brown crust made up of a complex mixture of iron oxide with clay minerals, owing to local weathering.

Petrography

The peridotite samples are variably serpentinized and generally composed of harzburgite and subordinate dunite. The degree of serpentinization is up to 40 vol. % in harzburgite and does not exceed 50 vol. % in dunite. In addition, completely serpentinized rocks originating from both peridotite types were also found. In serpentinized harzburgite, the primary mineral phases include olivine and orthopyroxene porphyroclasts accompanied by minor relicts of clinopyroxene and accessory Cr-spinel, whereas secondary phases include serpentine, chlorite and magnetite accompanied by minor tremolite and talc. Serpentinized dunite contains relicts of olivine, Cr-spinel and serpentine accompanied by subordinate chlorite and tremolite.

In the serpentinized peridotite matrix four different types of texture were recognized, in decreasing order of abundance: I) mesh texture defined by serpentine and magnetite that replace olivine, II) bastite texture represented by serpentine pseudomorphs after orthopyroxene, III) interpenetrating texture and IV) type-2 hourglass texture.

The mesh cores consist of serpentine, magnetite, chlorite (Fig. 2a) or olivine relicts, since replacement of olivine by serpentine and magnetite proceeds towards the olivine porphyroclast core. In some cases, outlines of large olivine crystals (> 1 mm) may be preserved in the groundmass of mesh-textured serpentinites after dunite, which indicates that dunites are mostly coarse-grained similarly to their harzburgitic equivalents. In the mesh rims, serpentine fibres are commonly perpendicularly oriented to the mesh cells. Bastite pseudomorphs are made up of serpentine (Fig. 2b), tremolite, chlorite or talc. They have elongated ovoidal shape and commonly exhibit Cr-spinel exsolution lamellae. Deformation characteristics such as kinking and undulatory extinction may still be recognizable at some bastite grains. Interpenetrating texture consists of elongated, intersecting blades of serpentine, whereas type-2 hourglass texture exhibits wavy extinction due to recrystallization (Fig. 2c; O'Hanley & Wicks 1995). In some samples these non-pseudomorphic textures are superimposed on the pseudomorphic ones (mesh and bastite).

Except for serpentine the other secondary silicate phases replace mantle exsolved orthopyroxene and clinopyroxene crystals. Moreover, chlorite was also found to form either intergrowths with serpentine or aureoles surrounding Cr-spinel grains. In the last case, chlorite is subhedral and bladed in shape and it was found to overprint mesh serpentine. Apart from replacing pyroxenes, tremolite also occurs as randomly oriented prismatic crystals scattered in the serpentinized groundmass. Magnetite commonly forms irregular networks (Fig. 2d) or occurs as fine dusty grains scattered in the serpentinized matrix. In some samples magnetite is overgrown on Cr-spinel grains (Fig. 2e), which represents textural evidence supporting its formation during serpentinization (syn-serpentinization magnetite).

Spinel textures

Cr-spinel constitutes less than 2–3 vol. % of the studied rocks. It occurs as isolated and fractured crystals in the peridotite groundmass. Grain sizes vary within samples, but most are between 0.1 and 1.5 mm. They appear to form red to dark brown coloured anhedral to subhedral crystals. Moreover, optical microscopy revealed that several Cr-spinel

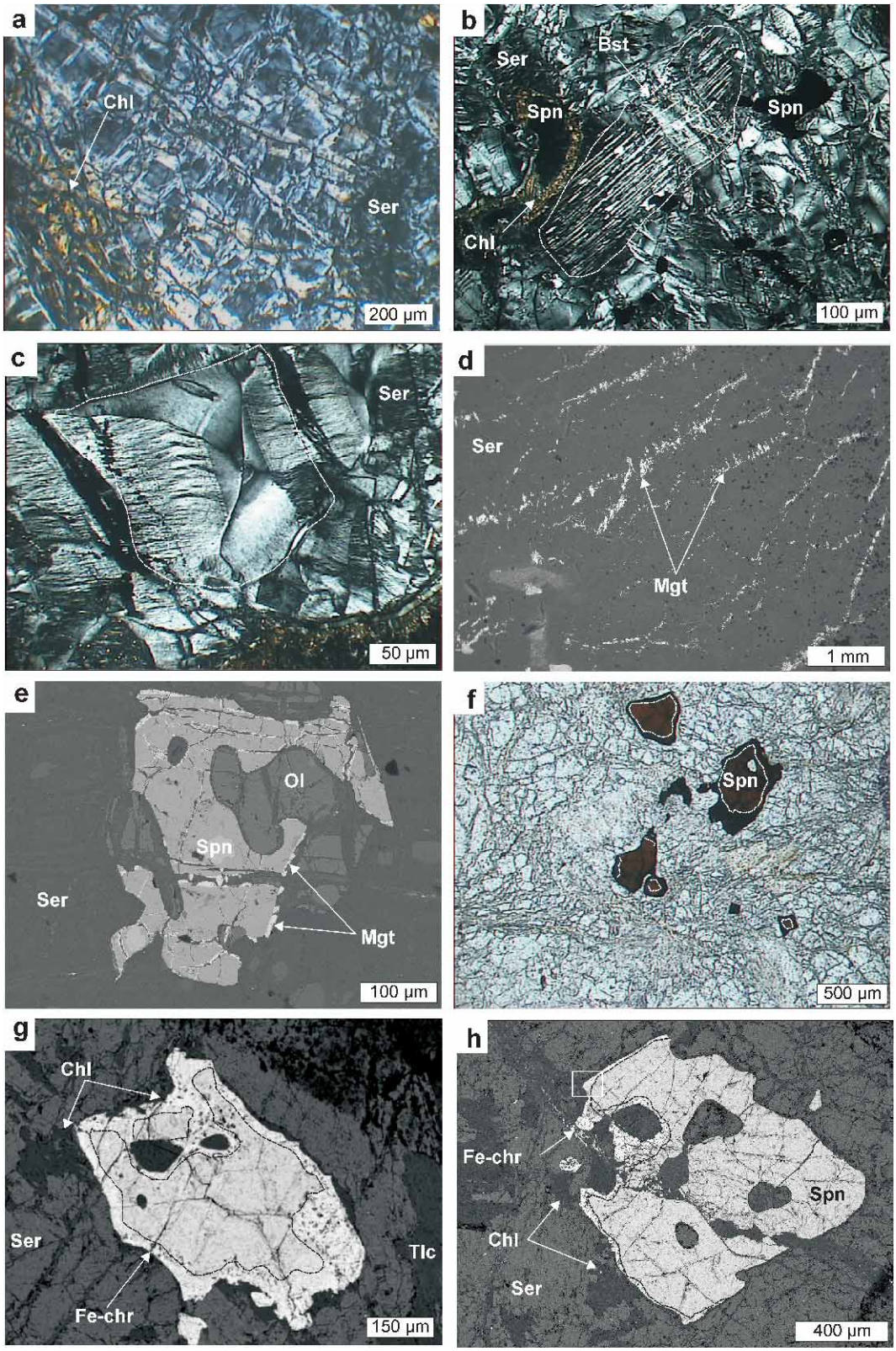

Fig. 2. a — Mesh texture (crossed nicols/XPL); **b** — Bastite texture marked by the white dashed line (XPL); **c** — Type-2 hourglass texture marked by the white dashed line (XPL); **d** — Magnetite network in serpentinized peridotite (back-scattered electron image/BSE); **e** — Syn-serpentinization magnetite overgrown on unaltered anhedral Cr-spinel (BSE); **f** — Cr-spinels exhibiting optical zoning (plane polarized nicols/PPL); **g** — Complete ferrian chromite rim in a Cr-spinel grain armoured by clinochlore aureole (BSE, micrograph taken from Kapsiotis et al. 2007). **h** — Partly altered Cr-spinel grain. **Abbreviations:** Ser — serpentine, Chl — clinochlore, Spn — Cr-spinel, Mgt — magnetite, Bst — bastite, Ol — olivine, Fe-Chr — ferrian chromite, Tlc — talc.

grains were optically inhomogeneous (Fig. 2f). Most of them show irregular zoning due to replacement by an opaque phase along cracks and grain boundaries. In petrographic terms only Cr-spinels in contact with chlorite display zoning. On the other hand, Cr-spinel grains solely in contact with serpentine are homogeneous.

Combined electron microscopy and mineral chemistry analytical work revealed that the opacity of the studied Cr-spinels is mainly correlated with an increase in their Fe^{2+} content. Their compositional zoning is apparent in back-scattered electron images (BSE), in which the edges of the zoned Cr-spinel grains appear to be bright and separated from the inner part of the grains by sharp contacts. Zoning, although commonly limited, advances from grain boundaries and fractures towards the inner part of the grain, which gives the crystal edges the appearance of being ragged and poorly defined (Fig. 2g). On the other hand, a few grains exhibiting patchy zoning were also found (Fig. 2h). Generally, the opaque zones have a porous structure displaying sieve texture. Analytical work revealed that the most sizeable pores are filled with chlorite. Intriguingly each zoned Cr-spinel is surrounded by chlorite aureoles (Fig. 2g). These aureoles are up to 70 μm thick and display grey to purple colours under cross-polarizers.

It is worthy mentioning that the extent of Cr-spinel zoning is not directly correlated with the degree of serpentinization of the host rocks. Even though harzburgite is generally less altered compared to dunite, harzburgitic Cr-spinels display zoning more frequently. Moreover, zoning extent and thickness are greater in Cr-spinels hosted in harzburgite. However, there are samples in which some accessory Cr-spinels may display zoning and some others not. Additionally, no zoning effect was observed in accessory Cr-spinel from 3 serpentinized dunite samples.

Analytical techniques

Cr-spinels were investigated *in situ* and imaged using a Super JEOL JSM–6300 scanning electron microscope (SEM) at the University of Patras, Greece. The quantitative analyses of Cr-spinel core–rim pairs, serpentine and chlorite (clinochlore) were performed using a Super JEOL JSM-6300 microprobe operated in wavelength-dispersive spectrometry (WDS) mode. Its operating conditions were 15 kV accelerating voltage and 20 nA beam current, with 4 μm beam diameter. The ZAF correction software was put into use (Reimer 1998). Calibrations were done using natural and synthetic reference materials. The proportion of Fe^{3+} in Cr-spinel was calculated assuming ideal spinel stoichiometry (AB_2O_4). 27 Cr-spinel and ferrian chromite pair analyses (19 from harzburgite and 8 from dunite) were carried out on 14 serpentinized mantle rock samples. Selected pair analyses of Cr-spinel and ferrian chromite from the studied serpentinized peridotites are listed in Table 1, whereas representative analyses of serpentine and clinochlore are listed in Table 2. Selected spinel-group minerals and clinochlore analytical data are taken from Kapsiotis et al. (2007).

Qualitative X-ray powder diffraction (XRD) analyses were performed using a Philips PW 1410 powder diffractometer to better characterize serpentine minerals. Powdered samples were scanned from 3 to 60° 2θ, with a step size of 0.02° 2θ and a count time of 4 sec per step.

Mineral chemistry (and XRD data)

Cr-spinel

Analytical traverses across optically zoned Cr-spinel grains revealed detectable chemical zoning. In serpentinized rocks from both areas Cr-spinel cores have quite similar compositions. In particular, Cr-spinel cores have Cr#[Cr/(Cr+Al)] that ranges between 0.45 and 0.73, and Mg#[Mg/(Mg+Fe^{2+})] that varies between 0.52 and 0.65 (Fig. 3a), thus they can

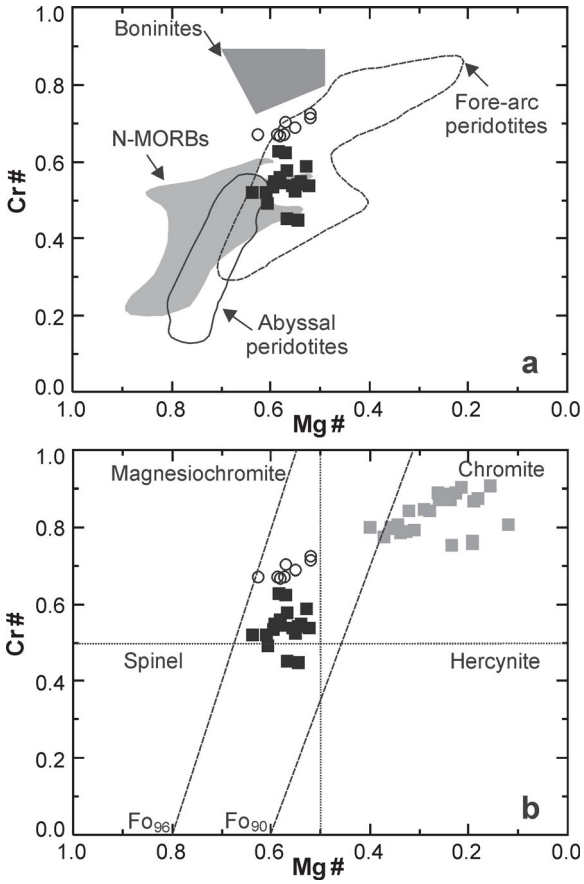

Fig. 3. Compositional variations of Cr-spinel cores and ferrian chromite from the studied serpentinized peridotites in terms of: **a** — Cr#[Cr/(Cr+Al)] versus Mg#[Mg/(Mg+Fe^{+2})]. Data for spinel in modern abyssal peridotites are from Dick & Bullen (1984) and Juteau et al. (1990). Field for spinel in equilibrium with boninites and N-MORB's is taken from Dick & Bullen (1984). Data for spinel in fore-arc peridotites are from Ishii et al. (1992) and Ohara & Ishii (1998). **b** — Classification of the composition of Cr-spinel and ferrian chromite from the studied peridotites in terms of Cr#[Cr/(Cr+Al)] versus Mg#[Mg/(Mg+Fe^{+2})]. Cr-spinel composition is also contoured at a nominal temperature of 1200 °C for olivine compositions from Fo_{90} to Fo_{96} (quantitatively computed by Dick & Bullen 1984). **Symbols:** black squares — harzburgitic Cr-spinel cores, open circles — dunitic Cr-spinel cores, grey squares — ferrian chromite.

Table 1: Representative electron-microprobe analyses of Cr-spinel and ferrian chromite pairs from the studied serpentinized peridotites (wt. % — not detected, Spn — Cr-spinel, Fe-chr — ferrian chromite). *Continued on the next page.*

Rock	Harzburgite																	
Area	Milia							Pefki										
Sample	M_1	M_1	PM_5	PM_5	PM_5	PM_{10}	PM_{10}	P_8	P_8	P_{15}	P_{15}	P_{17}	P_{17}	P_{17}	P_{17}	P_{17}	P_{17}	P_{17}
Mineral	Spn	Fe-chr	Spn	Fe-chr	Spn	Fe-chr	Spn	Spn	Fe-chr	Spn	Fe-chr	Spn	Fe-chr	Spn	Fe-chr	Spn	Fe-chr	Spn
Analysis	1core	1rim	1core	1rim	2core	2rim	1core	1core	1rim	1core	1rim	1core	1rim	2core	1rim	2core	2rim	2core
SiO_2	–	0.64	0.12	1.64	0.32	2.39	–	–	0.39	–	0.58	–	0.21	–	0.41	–	0.41	–
TiO_2	–	0.22	–	0.18	0.04	0.36	–	0.05	0.19	–	0.14	–	0.07	0.06	0.17	0.06	0.17	0.06
Al_2O_3	24.13	10.78	28.08	9.87	25.74	9.10	31.27	24.92	6.78	23.14	8.94	24.53	9.34	24.89	8.98	24.89	8.98	24.89
Cr_2O_3	42.66	49.89	40.23	50.46	41.38	52.06	37.84	44.77	53.45	47.44	52.98	44.58	51.67	44.65	51.94	44.65	51.94	44.65
Fe_2O_3	4.15	5.45	1.68	6.45	3.43	3.31	0.02	0.24	8.81	0.96	7.46	1.32	8.16	1.10	8.01	1.10	8.01	1.10
FeO	17.75	27.47	15.67	23.31	13.93	25.61	18.03	16.16	22.63	16.97	23.02	15.74	23.00	16.05	22.76	16.05	22.76	16.05
MnO	–	1.56	–	0.89	0.42	1.78	0.33	0.40	1.88	–	0.44	0.46	1.11	0.23	1.03	0.23	1.03	0.23
MgO	11.94	3.65	13.56	7.71	14.43	6.43	12.10	12.54	6.03	12.45	7.22	12.76	6.27	12.88	6.71	12.88	6.71	12.88
ZnO	–	–	–	–	–	–	–	–	0.28	–	–	–	0.38	–	0.44	–	0.44	–
Total	100.64	99.67	99.34	100.51	99.68	101.04	99.58	99.08	100.44	100.96	100.79	99.39	100.16	99.86	100.45	99.86	100.45	99.86
Atoms pfu based on O = 4																		
Si	–	0.022	0.004	0.055	0.010	0.080	–	0.039	–	0.013	–	0.020	–	0.007	–	0.014	–	0.014
Ti	–	0.006	–	0.005	0.001	0.009	–	0.004	0.001	0.005	–	0.004	–	0.002	0.001	0.004	0.001	0.004
Al	0.871	0.439	0.997	0.388	0.915	0.359	1.104	0.374	0.903	0.275	0.833	0.355	0.887	0.375	0.895	0.359	0.895	0.359
Cr	1.033	1.363	0.958	1.331	0.986	1.379	0.896	1.354	1.089	1.455	1.145	1.410	1.082	1.392	1.077	1.393	1.077	1.392
Fe^{+3}	0.096	0.142	0.038	0.162	0.078	0.083	–	0.186	0.006	0.233	0.022	0.189	0.031	0.215	0.025	0.212	0.025	0.215
Fe^{+2}	0.455	0.794	0.395	0.651	0.351	0.717	0.451	0.655	0.416	0.647	0.433	0.648	0.404	0.649	0.410	0.638	0.410	0.649
Mn	–	0.046	–	0.025	0.011	0.051	0.008	0.052	0.010	0.055	–	0.013	0.012	0.032	0.006	0.030	0.006	0.032
Mg	0.545	0.188	0.609	0.384	0.649	0.321	0.540	0.335	0.575	0.310	0.567	0.362	0.584	0.318	0.586	0.339	0.586	0.318
Zn	–	–	–	–	–	–	–	–	–	0.007	–	–	–	0.010	–	0.011	–	0.010
Cation sum	3.000	3.000	3.000	3.000	3.000	3.000	3.000	3.000	3.000	3.000	3.000	3.000	3.000	3.000	3.000	3.000	3.000	3.000
Cr#	0.54	0.76	0.49	0.77	0.52	0.79	0.45	0.78	0.55	0.84	0.58	0.80	0.55	0.79	0.55	0.80	0.55	0.79
Mg#	0.55	0.19	0.61	0.37	0.65	0.31	0.55	0.34	0.58	0.32	0.57	0.36	0.59	0.33	0.59	0.35	0.59	0.33
Fe^{3+}#	0.048	0.073	0.019	0.086	0.039	0.046	–	0.097	0.003	0.119	0.011	0.097	0.016	0.108	0.013	0.108	0.013	0.108

be classified as spinel to magnesiochromite solid solution members (Fig. 3b). Moreover, $Fe^{3+}/(Fe^{3+}+Fe^{2+})$ is up to 0.30. Cr_2O_3 ranges between 37.82 and 55.56 wt. %, Al_2O_3 between 14.12 and 31.27 wt. %, MgO between 10.78 and 14.13 wt. %, and FeO^t between 15.87 and 26.06 wt. %. In terms of Cr# and Mg# values Cr-spinel core analyses plot mostly in the field of spinel from fore-arc peridotites (Fig. 3a; Ishii et al. 1992; Ohara & Ishii 1998), whereas a few analyses plot on the boundary between the fields of spinel form fore-arc peridotites and abyssal peridotites (Fig. 3a; Dick & Bullen 1984; Juteau et al. 1990). Furthermore, Cr# is lower in Cr-spinel from harzburgite (0.45–0.63) compared to dunite (0.67–0.73; Fig. 3a).

On the other hand, the composition of opaque regions varies within the following ranges: Cr# = 0.75–0.90, Mg# = 0.12–0.40, which is indicative of chromite chemistry (Fig. 3b), while $Fe^{3+}/(Fe^{3+}+Fe^{2+}) < 0.55$. Cr_2O_3 ranges between 34.10 and 63.82 wt. %, Al_2O_3 between 4.02 and 11.07 wt. %, MgO between 2.27 and 8.05 wt. %, and FeO^t between 26.21 and 56.04 wt. %.

The TiO_2 content of Cr-spinel cores is generally very low (<0.11 wt. %), whereas it can be up to 0.48 wt. % in the porous opaque regions. MnO and SiO_2 contents are also lower in cores (<0.46 wt. % and <0.32 wt. %, respectively) compared to the rims (<1.88 wt. % and <2.39 wt. %). Moreover, $Fe^{3+}\#[Fe^{3+}/(Fe^{3+}+Cr+Al)]$ is low (<0.12), commonly showing a slight increase from core to rim. However, in two rims it was found to be relatively elevated (0.38 and 0.40).

Regarding certain mineral chemistry features (elevated FeO^t and reduced Al_2O_3 and MgO contents) combined with their physical properties (high reflectivity and low hardness), it can be claimed that the opaque regions correspond to a FeO^t- and Cr_2O_3-rich, Al_2O_3-poor spinel phase generally known as ferrian chromite.

Table 1: *Continued.*

Rock	Dunite											
Area	Milia								Pefki			
Sample	M_{2B}	M_{2B}	M_{2B}	M_{2B}	PM_{12}	PM_{12}	PM_{12}	PM_{12}	P_{11}	P_{11}	P_{11}	P_{11}
Mineral	Spn	Fe-chr	Spn	Fe-chr	Spn	Fe-chr	Spn	Fe-chr	Spn	Fe-chr	Spn	Fe-chr
Analysis	1core	1rim	3core	3rim	1core	1rim	2core	2rim	1core	1rim	3core	3rim
SiO_2	–	0.36	–	0.24	–	1.57	0.16	0.96	–	0.94	–	0.13
TiO_2	–	–	–	–	–	0.22	–	0.27	0.06	0.24	–	0.10
Al_2O_3	16.55	7.03	16.71	7.24	14.95	4.95	14.12	5.11	16.49	5.05	17.56	5.23
Cr_2O_3	49.94	58.08	50.45	57.98	55.55	58.98	55.56	59.01	54.57	59.65	52.75	59.01
Fe_2O_3	6.04	4.74	4.24	4.43	1.38	2.79	0.90	3.74	0.07	2.73	2.06	4.63
FeO	14.10	24.99	15.41	25.08	17.93	26.30	17.73	26.38	16.93	26.88	16.06	25.46
MnO	0.23	0.23	0.12	0.28	–	1.13	0.05	0.85	–	0.91	–	0.79
MgO	13.27	5.71	12.34	5.45	10.93	5.23	10.78	4.89	11.57	4.41	12.44	4.43
ZnO	–	–	–	–	–	–	–	–	–	–	–	–
Total	100.12	101.13	99.26	100.69	100.74	101.17	99.30	101.21	99.69	100.80	100.88	99.77
Atoms pfu based on O = 4												
Si	–	0.012	–	0.008	–	0.054	0.005	0.033	–	0.033	–	0.005
Ti	–	–	–	–	–	0.006	–	0.007	0.001	0.006	–	0.003
Al	0.614	0.283	0.628	0.293	0.563	0.201	0.541	0.208	0.620	0.207	0.647	0.217
Cr	1.243	1.570	1.271	1.576	1.404	1.607	1.427	1.614	1.376	1.643	1.304	1.645
Fe^{+3}	0.143	0.122	0.102	0.115	0.033	0.072	0.022	0.097	0.002	0.071	0.049	0.123
Fe^{+2}	0.371	0.715	0.411	0.721	0.479	0.758	0.482	0.763	0.451	0.783	0.420	0.751
Mn	0.006	0.007	0.003	0.008	–	0.033	0.001	0.025	–	0.027	–	0.024
Mg	0.623	0.291	0.586	0.279	0.521	0.269	0.522	0.252	0.550	0.229	0.580	0.233
Zn	–	–	–	–	–	–	–	–	–	–	–	–
Cation sum	3.000	3.000	3.000	3.000	3.000	3.000	3.000	3.000	3.000	3.000	3.000	3.000
Cr#	0.67	0.85	0.67	0.84	0.71	0.89	0.73	0.89	0.69	0.89	0.67	0.88
Mg#	0.63	0.29	0.59	0.28	0.52	0.26	0.52	0.25	0.55	0.23	0.58	0.24
Fe^{3+}#	0.072	0.062	0.051	0.058	0.017	0.038	0.011	0.051	0.001	0.037	0.025	0.062

Table 2: Representative electron-microprobe analyses of serpentine and clinochlore from the studied peridotites (wt. % — not detected; analyses PM11/1 and P22/1 are taken from Kapsiotis et al. 2007).

Area	Milia			Pefki				Milia		Pefki		
Sample	PM_{2A}	PM_{2A}	PM_5	P_{15}	P_{16}	P_{21}	P_{22}	PM_{2A}	PM_{11}	P_{21}	P_{21}	P_{22}
Mineral	Serpentine							Clinochlore				
Analysis	1	2	8	6	2	2	1	1	1	4	5	1
SiO_2	44.55	44.04	39.69	41.79	40.64	40.18	40.9	30.04	34.85	34.24	35.37	37.15
TiO_2	0.18	–	0.17	–	–	–	0.05	–	–	–	–	–
Al_2O_3	1.20	0.54	0.54	0.04	0.17	0.86	0.32	21.07	13.06	18.85	16.75	9.64
Cr_2O_3	0.40	0.17	–	–	–	0.54	–	0.29	3.33	2.45	2.02	2.37
FeO_t	2.20	1.32	5.39	7.29	7.74	7.51	6.57	5.38	1.42	3.05	3.16	3.47
MgO	41.00	36.83	35.76	39.36	37.01	34.75	35.32	28.04	33.14	33.34	34.63	34.52
NiO	–	0.17	–	0.59	0.23	–	0.21	0.06	0.22	0.16	–	0.42
MnO	0.34	–	0.42	0.08	0.03	–	–	0.01	–	0.10	–	–
CaO	–	0.15	0.08	–	–	–	–	–	0.05	–	–	–
Na_2O	–	0.44	–	–	–	–	–	–	–	–	–	–
K_2O	–	0.69	–	–	–	–	–	–	–	–	–	–
Total	89.87	84.35	82.05	89.15	85.82	83.84	83.37	84.89	86.07	92.19	91.93	87.57
Atoms pfu based on O (+ OH) = 9								Atoms pfu based on O = 28				
Si	2.001	2.100	1.978	1.936	1.952	1.970	2.007	5.840	6.613	6.099	6.307	6.988
Al^{IV}	–	–	0.022	0.002	0.010	0.030	–	2.160	1.387	1.901	1.693	1.012
Al^{VI}	0.063	0.030	0.010	–	–	0.020	0.018	2.664	1.531	2.053	1.824	1.123
Ti	0.006	–	0.006	–	–	–	0.002	–	–	–	–	–
Cr	0.014	0.006	–	–	–	0.021	–	0.045	0.499	0.345	0.284	0.352
Fe^{+3}	0.070	0.050	0.20	0.250	0.280	0.280	0.240	–	–	–	–	–
Fe^{+2}	–	–	–	–	–	–	–	0.875	0.225	0.454	0.471	0.546
Ni	–	0.010	–	0.020	0.010	–	0.010	0.010	–	0.020	–	0.060
Mn	0.013	–	0.018	0.003	0.001	–	–	0.002	–	0.015	–	–
Mg	2.745	2.618	2.657	2.718	2.651	2.539	2.583	8.126	9.293	8.854	9.206	9.680
Ca	–	0.008	0.004	–	–	–	–	–	–	–	–	–
Na	–	0.041	–	–	–	–	–	–	–	–	–	–
K	–	0.042	–	–	–	–	–	–	–	–	–	–
Cation sum	4.912	4.905	4.895	4.929	4.904	4.860	4.860	19.722	19.746	19.741	19.785	19.761

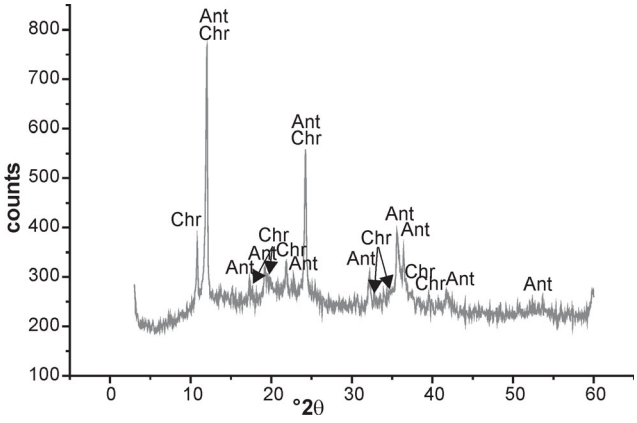

Fig. 4. X-ray diffraction (XRD) diagram showing the presence of antigorite and chrysotile polymorphs in the studied serpentinized peridotites. **Abbreviations:** Ant — antigorite, Chr — chrysotile.

Serpentine

As it was identified by XRD data, the serpentine groundmass of the studied hydrated peridotites consists of antigorite and chrysotile (Fig. 4). Antigorite was found to be the dominant serpentine polymorph in interpenetrating and type-2 hourglass texture. Most of serpentine grains contain relatively elevated concentrations of Al_2O_3 (up to 2.37 wt. %), consistently with antigorite composition. SiO_2 ranges between 41.94 and 46.67 wt. %, MgO between 35.71 and 42.04 wt. %, whereas Cr_2O_3 is up to 0.88 wt. %. Chrysotile grains contain lower Al_2O_3 (up to 0.46 wt. %), whereas Cr_2O_3 content is below the detection limit of the electron microprobe.

Chlorite

Chlorites are characterized by relatively high Cr_2O_3 (up to 3.33 wt. %). Their SiO_2 content varies between 30.04 and 37.15 wt. %, whereas Al_2O_3 concentration may be up to 21.07 wt. % and MgO content ranges between 28.04 and 34.63 wt. %. Concentrations of TiO_2, MnO and NiO are low and sometimes even below detection limits. The Si contents of chlorite classify them as clinochlore after the classification of Bailey (1980). Their chemical characteristics are similar to those of chlorites from other hydrated ophiolitic peridotites (e.g. Jan & Windley 1990).

Discussion

Primary Cr-spinel compositions

The compositions of Cr-spinel cores are generally similar within individual samples. They are characterized by moderate to elevated Cr#(0.45–0.73), high Mg#(0.52–0.65), low Fe^{3+}# resembling in composition Cr-spinels in podiform chromitites from the Rayat area, northeastern Iraq (Arai et al. 2006). In addition, their TiO_2 and MnO contents are low (<0.11 wt. % and <0.46 wt. %, respectively), which is rather usual for unaltered Cr-spinel in ultramafic rocks (e.g. Barnes 2000; Singh & Singh 2013). Cr-spinel cores should form at high *T's* in equilibrium with olivine containing ~Fo_{93}, since their composition runs between the Fo_{90} and Fo_{96} contours (Fig. 3b). Moreover, Cr-spinel core compositions plot outside of the fields of metamorphic spinel compositions (Fig. 5), which further implies that they have not been affected by post-magmatic processes and retain their primary composition. Therefore, they can be used as indicators to unravel the petrogenesis of peridotites.

The composition of accessory Cr-spinel in peridotites is regarded as a useful tool for revealing melting processes in the mantle (e.g. Okamura et al. 2006; Uysal et al. 2007). It is known that Cr# of spinel is sensitive to melting processes and that systematically increases with the degree of peridotite depletion (e.g. Zhou et al. 2005; Uysal et al. 2012). Based on that criterion it is deduced that the studied peridotites were produced by variable degrees of mantle melting and that dunite represents a mantle residue resulting from higher melting degrees compared to harzburgite.

Except for partial melting, melt-peridotite interaction process may account for the high Cr# values in spinel (e.g. Uysal et al. 2012). In contrast to metasomatically added Cr-spinel grains the studied ones are commonly anhedral to subhedral in shape and depleted in TiO_2, which are suggestive of their residual origin. Additionally, Cr-spinels analysed in the present study bear no compositional similarities with spinel in equilibrium with boninite melts. On the other hand, a few analyses plot on the boundary of the field representing the composition of spinel in equilibrium with normal mid ocean ridge basalts (N-MORBs, Fig. 3a). However, a MORB melt would crystallize spinels having low Cr# (<0.60) and elevated TiO_2. Therefore, any magmatic/metasomatic origin of the examined Cr-spinels should be precluded.

It has been established that Cr-spinel composition can reflect formation of mantle rocks in different tectonic regimes (e.g. Zhou et al. 2005; Ahmed et al. 2012). According to a number of studies Cr-spinels with Cr#<0.60 are commonly found in abyssal peridotites related to the lithospheric mantle emplaced near the ocean ridge, whereas those having higher values are found in peridotites produced in a supra-subduction zone (SSZ) environment (e.g. Dick & Bullen 1984; Juteau et al. 1990; Ishii et al. 1992; Ohara & Ishii 1998). In such settings, fluid assisted partial melting leads to higher peridotite melting degrees, thereby elevating Cr# in Cr-spinel (e.g. González-Jiménez et al. 2011; Derbyshire et al. 2013). In terms of Cr# *vs* Mg# values the majority of Cr-spinel analyses plot in the field of spinel from fore-arc peridotites (Fig. 3a). On the other hand, a few harzburgitic Cr-spinel analyses plot near the intersection of spinel fields form fore-arc peridotites and modern abyssal peridotites (Fig. 3a), thus indicating that they represent hybrid mineral compositions.

The compositional features of Cr-spinels from the Pindos peridotites indicate that these rocks were probably affected by a two-stage melting process, including: 1) a partial melting episode in a mid ocean ridge (MOR) setting, recorded in residual harzburgites with low Cr# (<0.60) Cr-spinels, 2) followed by subsequent entrapment and melting of harzburgites in the mantle wedge above an intra-oceanic SSZ. The latter melting episode is documented by the existence of high Cr#

(>0.60) Cr-spinels in both peridotite types and was most likely responsible for the formation of dunites.

Origin of zoning in Cr-spinel: implications for the post-magmatic evolution of peridotites

Zoning in Cr-spinel might originate as a result of various processes. For instance in cumulate rocks zoning in Cr-spinel may be the product of reactions with the intercumulus liquid (e.g. Saumur & Hattori 2013). However, the studied serpentinized ultramafic rocks represent hydrated residual mantle peridotites, having petrographic and mineral chemistry features inconsistent with a cumulate origin. On the other hand, the examined peridotites could have reacted with mafic melts produced by fluid assisted partial melting of the mantle wedge above a subducted slab. Melt-peridotite interaction may produce zoning patterns in accessory Cr-spinel (e.g. Mondal & Zhou 2010). However, there is no textural evidence to support such a possibility and as was discussed above, the studied Cr-spinels are supposed to have a residual origin.

Textural evidence indicates that the zoning pattern in Cr-spinel is not a primary feature. In fact, it is apparently related to the post-magmatic processes by which the peridotites were affected since zoned Cr-spinel occurs exclusively in altered rock samples. However, it is not clear which process, serpentinization or regional metamorphism, is responsible for the alteration of Cr-spinel. The investigated peridotites are not uniformly serpentinized. Moreover, zoning is not so common in accessory Cr-spinel from serpentinized dunite. In addition, Cr-spinels bordered by serpentine do not exhibit any alteration marks. Furthermore, the common finding of clinochlore aureoles surrounding zoned Cr-spinel and overprinting mesh serpentine provides evidence that the crystallization of clinochlore post-dated serpentinization. Equally, clinochlore in the examined hydrated peridotites contains higher Al_2O_3, Cr_2O_3 and Mg/Fe compared to those in olivine or pyroxene, thus it could not have formed by isochemical replacement of these silicate phases during serpentinization.

According to a number of recent researches Cr-spinel remains almost unaffected during serpentinization, although it becomes variably altered during low-grade metamorphism (e.g. Mellini et al. 2005; Mikuš & Spišiak 2007; Farahat 2008; González-Jiménez et al. 2009; Merlini et al. 2009; Gervilla et al. 2012; Singh & Singh 2013). According to Bach et al. (2006) common low-*T* serpentinization, taking place during ocean-floor metamorphism cannot cause any changes in Cr-spinel composition. Furthermore, Merlini et al. (2009) suggest that Cr-spinels that were not subjected to any higher-*T* metamorphic overprints after serpentinization retain their mantle/igneous composition. In addition, Barnes (2000) suggested that only prograde metamorphism might have a significant impact on Cr-spinel chemistry at a post-magmatic stage of evolution.

Overall observations indicate that Cr-spinel undergoes dissolution along fractures and grain boundaries, being partially replaced by ferrian chromite. Although well-developed clinochlore growths are common adjacent to the altered parts of Cr-spinel grains, zoning in the latter is texturally limited to their boundaries and fractures. The irregular development of ferrian chromite along grain boundaries and fractures further indicates that no crystallographic orientation has been followed for its formation and that alteration is heterogeneous even on grain scale. Moreover, it indicates that alteration process had not occurred uniformly from all directions (e.g. Bliss & MacLean 1975; Mukherjee et al. 2010). Thus, textural evidence suggests that the alteration rims of zoned Cr-spinel represent only the initial stages of its compositional modification. According to Candia & Gaspar (1997) complete metamorphic re-equilibration takes place only when $P_{H_2O}=P_{total}$. Under $P_{H_2O}<P_{total}$, relict primary textures are preserved. Moreover, Merlini et al. (2009) suggested the following reaction for ferrian chromite formation: $2(Mg_{0.60}Fe_{0.40})(Cr_{1.30}Al_{0.70})O_4+3/2(Mg_{2.57}Al_{0.32}Fe_{0.11})Si_2O_5(OH)_4+H_2O+1/12O_2 \rightarrow 7/6(Mg_{0.40}Fe_{0.60})(Cr_{1.85}Fe_{0.08}Al_{0.07})O_4+1/2(Mg_{9.18}Fe_{0.34}Al_{1.60}Cr_{0.88})(Al_2Si_6)O_{20}(OH)_{16}$, and supported that replacement of Cr-spinel by ferrian chromite is commonly partial, because the reaction between Cr-spinel and serpentine during metamorphism does not convert all of the reactants and the environment acts as a closed system with the exception of fluids. Cr-spinel textures show that the initial size of the grains remained unchanged after alteration. However, a mass loss took place during ferrian chromite formation (indicated by the reaction above) resulting in the formation of pores.

The occurrence of ferrian chromite in hydrated forearc mantle peridotites is very rare (e.g. Tsujimori et al. 2004; Saumur & Hattori 2013). On the other hand, the formation of ferrian chromite in serpentinites requires heating after serpentinization (e.g. Cerny 1968). Although high-*T* phases, such as antigorite, tremolite and talc are present in the studied hydrated peridotites, the presence of texturally 'immature' ferrian chromite is in accordance with affection of peridotites by a short-lived thermal event, which did not allow complete development of thick ferrian chromite rims. The occurrence of ferrian chromite in the examined rocks indicates that they have been affected by a brief heating event uncommon in cases of typical serpentinite exhumation. Field observations support that serpentinites display foliation along well-developed shear zones, which provides further evidence that the studied peridotites were affected by regional metamorphism. These shear zones have been developed during the upward protrusion of the investigated peridotites (Rassios & Moores 2006), from the base of the mantle wedge through its hotter interior towards cooler shallow crustal levels along major thrust zones. Probably the passage of these already hydrated peridotites through the hot mantle wedge interior caused a thermal event allowing ferrian chromite formation to take place.

Ferrian chromite formation

Cr-spinel replacement by secondary phases like ferrian chromite and Cr-magnetite is direct evidence that even Cr-Fe-oxides may become unstable in the post-magmatic environment (e.g. Farahat 2008; González-Jiménez et al. 2009; Mukherjee et al. 2010). Textural and compositional variations in the studied zoned Cr-spinel grains suggest that alteration to ferrian chromite took place after serpentinization.

During that metamorphic episode primary Cr-spinel (now preserved in the core of zoned Cr-spinels) lost Al_2O_3 and MgO, whereas it became enriched in FeO^t and residually in Cr_2O_3 (Fig. 5). Kimball (1990) suggested that during Cr-spinel breakdown, Cr is preferentially incorporated in Cr-spinel and Al in chlorite and that explains the higher Cr and lower Al content in altered spinel. Mg and Al are fixed in the coexisting layer silicates (chrysotile/antigorite) to promote the formation of clinochlore. In addition, the core has lower concentrations of MnO and SiO_2 compared to the rim (Fig. 5). Mn commonly substitutes for Fe^{2+} in Cr-spinel lattice (e.g. Singh & Singh 2013). However, Mn is more susceptible to leaching (Stanton 1972), thus MnO increase from core to rim is in accordance with Mn release from the surrounding olivine upon serpentinization (e.g. Barnes 2000). Furthermore, the SiO_2 content detected in ferrian chromite rims should be ascribed to septochlorite intergrowths within the pores (e.g. Mellini et al. 2005; Derbyshire et al. 2013). It is worth mentioning that although high ZnO contents may be common in altered Cr-spinel from metamorphosed ultramafic rocks (e.g. Barnes 2000; Singh & Singh 2013) the present ferrian chromite compositions are depleted in Zn. High Zn contents in ferrian chromite might be explained by Cr-spinel re-equilibration with olivine prior to serpentinization, because Zn is commonly concentrated in olivine. However, the olivine in the examined rocks does not contain ZnO (unpublished data), which further explains the absence of Zn from the ferrian chromite.

The examined ferrian chromite compositions differ from those commonly reported in the literature, especially in terms of Fe^{3+}#, which is suggestive of their compositional 'immaturity'. In the vast majority of the studied zoned Cr-spinels Fe^{3+}# shows a weak increase from core to rim, having low values (<0.12). However, two ferrian chromite analyses show higher Fe^{3+}# (0.38 and 0.40). Their slight Fe^{3+} enrichment suggests the local passage to relatively more oxidizing alteration conditions. Gervilla et al. (2012) claimed that Fe-bearing fluid circulation takes place in such conditions, assisted by the already formed interconnected network of pores in Cr-spinel, causing dissolution of the silicates (mainly chlorite) in the pores and promoting diffusion of Fe^{2+} and Fe^{3+} into ferrian chromite, according to the following reaction: $(Fe_{0.6}Mg_{0.4})Cr_2O_4 + Fe_3O_4 \rightarrow 2(Fe_{0.8}Mg_{0.2})CrFeO_4$. The present data suggest that the amount of magnetite component added in ferrian chromite was very restricted and the reaction proposed above remained incomplete.

Metamorphic evolution path

Projection of Cr-spinel analyses on the triangular diagram Al^{3+}–Cr^{3+}–Fe^{3+} indicates that ferrian chromite compositions plot mainly within the compositional field of Cr-spinel

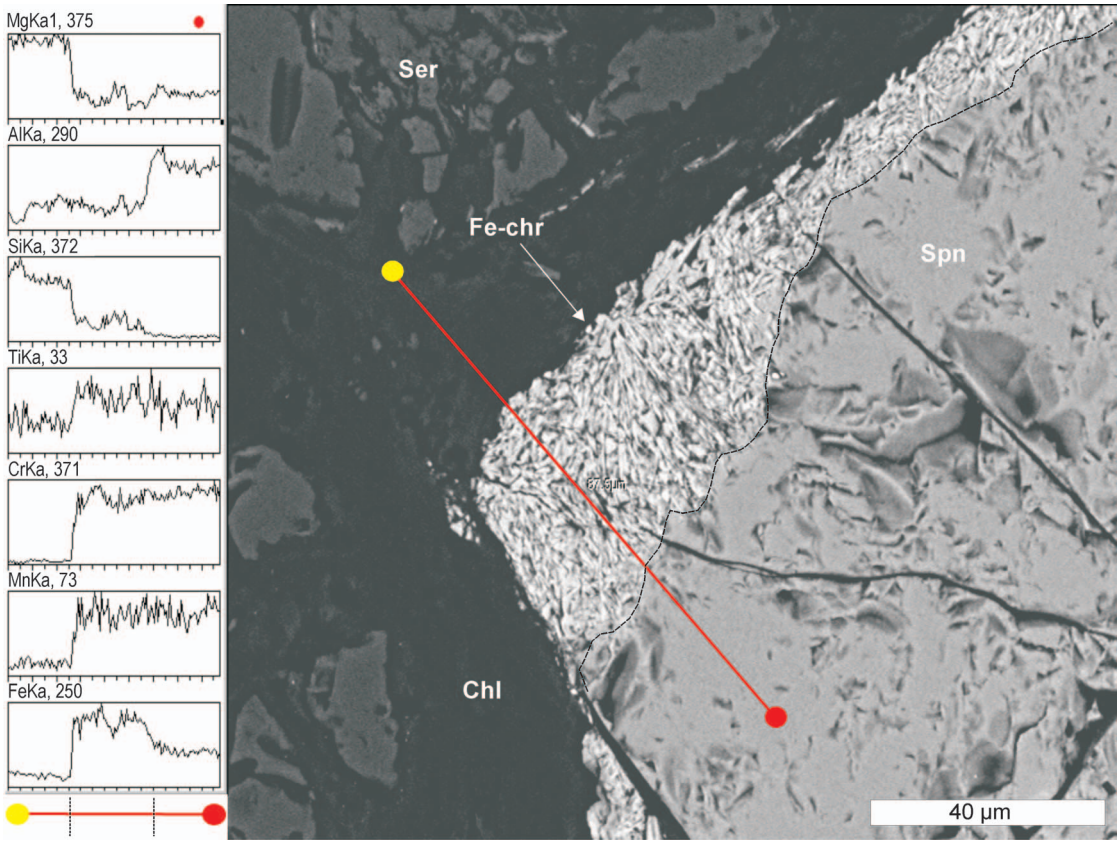

Fig. 5. BSE image (white square on Fig. 2h), showing limited Cr-spinel replacement by ferrian chromite (indicated by the black dashed line) and clinochlore and profile line analyses illustrating elemental variations between clinochlore, ferrian chromite and unaltered Cr-spinel. **Abbreviations:** Chl — clinochlore, Fe-chr — ferrian chromite, Ser — serpentine, Spn — Cr-spinel.

formed during the greenschist facies metamorphism (Fig. 6). In addition, two ferrian chromite analyses plot within the field of spinel affected by low amphibolite facies metamorphism. *T* is supposed to range between 200 and 400 °C during greenschist facies metamorphism (Ernst 1993). Moreover, according to Merlini et al. (2009) *T* needs to be strictly above 300 °C to allow metamorphism to provoke significant changes in Cr-spinel chemistry. The presence of tremolite and talc in the secondary assemblage of the Pindos hydrated peridotites provides direct evidence that *T* rose above 400 °C (Evans & Frost 1975) during metamorphism. Additionally, the occurrence of clinochlore/antigorite intergrowths in the altered silicate groundmass of the studied rocks, combined with the absence of metamorphic olivine (after dehydration of antigorite) implies that *T* did not exceed the range of lower amphibolite facies metamorphism (Caruso & Chernosky 1979).

Therefore, the following two-stage post-magmatic evolution scenario is proposed in order to explain Cr-spinel alteration in the Pindos serpentinized peridotites. During ocean-floor hydrothermal alteration, low *T* serpentinization did not produce any compositional or textural change in Cr-spinel, as it took place under reducing conditions (indicated by the low Fe^{3+}# values), probably at *T's* below 300 °C where chrysotile is stable (e.g. Schwartz et al. 2013). The second stage mainly has to do with the formation of ferrian chromite under higher *T* (>300 °C) hydrous fluid-saturated conditions, and involves the dissolution–precipitation reaction of primary Cr-spinel with serpentine to produce clinochlore and FeO- and Cr_2O_3-rich, Al_2O_3-poor Cr-spinel, according to the reactive mechanism proposed by Merlini et al. (2009). These hydrous MgO- and SiO_2-rich fluids (probably derived from first stage low-*T* serpentinization of olivine and pyroxene) had the opportunity to carry out element diffusion exchanges, promoting a compositional gradient across Cr-spinel grains, which is now being viewed as zoning. Cr-spinel and serpentine re-equilibration to form ferrian chromite and clinochlore, respectively, took place around the transition from mid- to advanced greenschist facies metamorphism (at *T's* > 300 °C), which is also supposed to stabilize antigorite.

Generally, the present ferrian chromite compositions indicate metamorphic alteration of Cr-spinel under elevated greenschist facies conditions. However, two ferrian chromite analyses, characterized by the highest Fe^{3+} contents (Fig. 6), are suggestive of more oxidizing conditions. These ferrian chromite compositions in the studied peridotites imply the passage to low-grade amphibolite facies metamorphism (550 °C < *T* < 600 °C). However, such metamorphic grade was only locally achieved, as it is indicated by the coincidental presence of ferrian chromite with high Fe^{3+}# values.

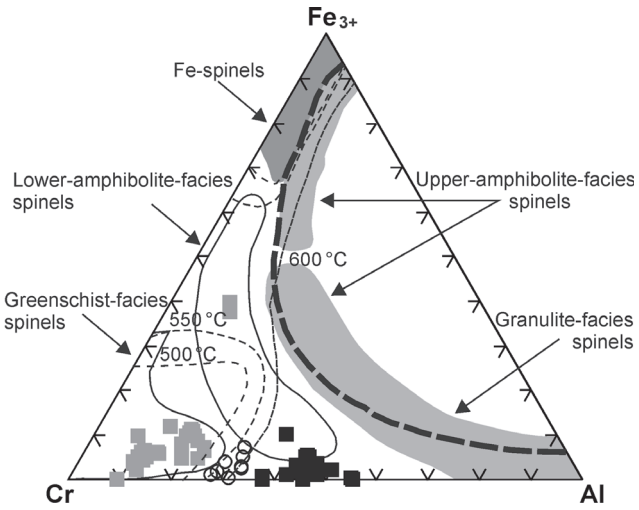

Fig. 6. Compositional changes in Cr-spinels from the Pindos serpentinized peridotites expressed in a triangular Al–Fe^{3+}–Cr plot with special reference to the fields of the different metamorphic facies defined for Cr-spinels by Purvis et al. (1972), Evans & Frost (1975) and Suita & Streider (1996). Solvus determined at 600, 550 and 500 °C by Shack & Ghiorso (1991) for chromite coexisting with olivine containing 90% forsterite. **Symbols:** black squares — harzburgitic Cr-spinel cores, open circles — dunitic Cr-spinel cores, grey squares — ferrian chromite.

Conclusions

Variably serpentinized peridotites occur in the Dramala Unit of the Pindos Ophiolite Complex in Greece. Accessory Cr-spinel in these rocks occasionally displays limited alteration to an opaque phase along fractures and grain boundaries. Cr-spinel cores preserve their primary composition, which further indicates that the studied rocks represent residual mantle peridotites that were produced by variable degrees of melting through a two-stage melting process, initiated in a MOR setting that was evolved in a SSZ. Cr-spinel is altered to a FeO- and Cr_2O_3-rich but MgO- and Al_2O_3-poor spinel phase, referred to as ferrian chromite, which is armoured by clinochlore overgrowing mesh serpentine. The extent and frequency of Cr-spinel replacement by ferrian chromite does not correlate with the degree of rock serpentinization and appears to be the result of a short-lived thermal event. Overall data show that alteration of Cr-spinel took place after serpentinization, mainly during an episode of advanced greenschist facies metamorphism.

Acknowledgments: This paper is based in part on the Ph.D. Thesis of A. Kapsiotis at the University of Patras, Greece. Drs. D. Lenaz, P. Uher and T. Mikuš are gratefully acknowledged for their constructive criticism on a preliminary version of the manuscript. Special thanks are also due to Dr. I. Broska for his editorial comments. The author is thankful to Dr. K. Hatzipanagiotou for his encouragement and those colleagues from the Department of Geology at the University of Patras who did not tire in sharing ideas. V. Kotsopoulos of the Laboratory of Electron Microscopy and Microanalysis, University of Patras, is also acknowledged for his assistance with the microanalyses and SEM micrographs. Research was partly supported by the University of Patras, 'K. Karatheodoris' program and Pythagoras I Project, which is co-funded by the European Social Fund and national resources (EPEAK). A. Kapsiotis was also supported by the State Scholarship Foundation of Greece (IKY) during his Ph.D. study.

References

Ahmed H.A., Harbi H.M. & Habtoor A.M. 2012: Compositional variations and tectonic settings of podiform chromitites and associated ultramafic rocks of the Neoproterozoic ophiolite at Wadi Al Hwanet, northwestern Saudi Arabia. *J. Asian Earth Sci.* 56, 118–134.

Arai S. 1992: Chemistry of chromian spinel in volcanic rocks as a potential guide to magma chemistry. *Mineral. Mag.* 56, 173–184.

Arai S., Shimizu Y., Ismail S.A. & Ahmed A.H. 2006: Low-*T* formation of high-Cr spinel with apparently primary chemical characteristics within podiform chromitite from Rayat, northeastern Iraq. *Mineral. Mag.* 70, 5, 499–508.

Arif M. & Jan M.Q. 2006: Petrotectonic significance of the chemistry of chromite in the ultramafic-mafic complexes of Pakistan. *J. Asian Earth Sci.* 27, 628–646.

Bach W., Paulick H., Garrido C.J., Ildefonse B., Meurer W. & Humphris S.E. 2006: Unravelling the sequence of serpentinization reactions: petrography, mineral chemistry, and petrophysics of serpentinites from MAR 15 °N (ODP Leg 209, Site 1274). *Geophys. Res. Lett.* 25, 1467–1470.

Bailey S.W. 1980: Summary of recommendations of AIPEA nomenclature committee on clay minerals. *Amer. Mineralogist* 65, 1–7.

Barnes S.J. 2000: Chromite in komatiites. II. Modification during greenschist to mid-amphibolite facies metamorphism. *J. Petrology* 41, 387–409.

Barnes S.J. & Roeder P.L. 2001: The range of spinel compositions in terrestrial mafic and ultramafic rocks. *J. Petrology* 42, 2279–2302.

Bliss N.W. & MacLean W.H. 1975: The petrogenesis of zoned chromite from central Manitoba. *Geochim. Cosmochim. Acta* 39, 973–990.

Burkhard D.J.M. 1993: Accessory chromium spinels: Their coexistence and alteration in serpentinites. *Geochim. Cosmochim. Acta* 57, 1297–1306.

Candia M.A.F. & Gaspar J.C. 1997: Chromian spinels in metamorphosed ultramafic rocks from Mangabal I and II complexes, Goiás, Brazil. *Miner. Petrology* 60, 27–40.

Caruso L.J. & Chernosky J.V. Jr 1979: The stability of lizardite. *Canad. Mineralogist* 17, 757–769.

Cerny P. 1968: Comments on serpentinization and related metasomatism. *Amer. Mineralogist* 53, 1377–1385.

Derbyshire E.J., O'Driscoll B., Lenaz D., Gertisser R. & Kronz A. 2013: Compositionally heterogeneous podiform chromitite in the Shetland Ophiolite Complex (Scotland): Implications for chromitite petrogenesis and late-stage alteration in the upper mantle portion of a supra-subduction zone ophiolite. *Lithos* 162–163, 279–300.

Dick H.J.B. & Bullen T. 1984: Chromian spinel as a petrogenetic indicator in abyssal and alpine-type peridotites and spatially associated lavas. *Contr. Mineral. Petrology* 86, 54–76.

Ernst W.G. 1993: Metamorphism of Franciscan tectonostratigraphic assemblage, Pacheco Pass area, east-central Diablo Range, California Coast Ranges. *Bull. Geol. Soc. Amer.* 105, 618–636.

Evans B.W. & Frost B.R. 1975: Chrome-spinel in progressive metamorphism. A preliminary analysis. *Geochim. Cosmochim. Acta* 39, 959–972.

Farahat E.S. 2008: Chrome-spinel in serpentinites and talc carbonates of the El Ideid-El Sodmein District, central Eastern Desert, Egypt: their metamorphism and petrogenetic implications. *Chem. Erde* 68, 193–205.

Gervilla F., Padrón-Navarta J.A., Kerestedjian T., Sergeeva I., González-Jiménez J.M. & Fanlo I. 2012: Formation of ferrian chromite in podiform chromitites from the Golyamo Kamenyane serpentinite, Eastern Rhodopes, SE Bulgaria: a two stage process. *Contr. Mineral. Petrology* 164, 643–657.

Ghikas C., Dilek Y. & Rassios A.E. 2009: Structure and tectonics of subophiolitic mélanges in the western Hellenides (Greece): implications for ophiolite emplacement tectonics. *Int. Geol. Rev.* 52, 423–453.

González-Jiménez J.M., Kerestedjian T., Proenza J.A. & Gervilla F. 2009: Metamorphism on chromite ores from the Dobromirtsi ultramafic massif, Rhodope mountains (SE Bulgaria). *Geol. Acta* 7, 413–429.

González-Jimenéz J.M., Proenza J.A., Gervilla F., Melgarejo J.C., Blanco-Moreno J.A., Ruiz-Sánchez R. & Griffin W.L. 2011: High-Cr and High-Al chromitites from the Sagua de Tánamo district, Mayarí-Cristal ophiolitic massif (eastern Cuba): Constraints on their origin from mineralogy and geochemistry of chromian spinel and platinum-group elements. *Lithos* 125, 101–121.

Grieco G. & Merlini A. 2012: Chromite alteration processes within Vourinos ophiolite. *Int. J. Earth Sci.* 101, 1523–1533.

Hellebrand E., Snow J.E., Dick H.J.B. & Hofmann A.W. 2001: Coupled major and trace elements as indicator of the extent of melting in mid-ocean-ridge peridotites. *Nature* 410, 677–681.

Ishii T., Robinson P.T., Maekawa H. & Fiske R. 1992: Petrological studies of peridotites from diapiric serpentinite seamounts in the Izu-Mariana fore-arc, Leg 125. *Proc. ODP, Sci. Res.* 125, 445–485.

Jan M.Q. & Windley B.F. 1990: Chromian spinel silicate chemistry in ultramafic rocks of the Jijal complex, northwestern Pakistan. *J. Petrology* 31, 667–715.

Jones G. & Robertson A.H.F. 1991: Tectono-stratigraphy and evolution of the Mesozoic Pindos ophiolite and related units, northwestern Greece. *J. Geol. Soc. London* 148, 267–288.

Jones G., Robertson A.H.F. & Cann J.R. 1991: Genesis and emplacement of the suprasubduction zone Pindos Ophiolite, northwestern Greece. In: Peters T., Nicolas A. & Coleman S. (Eds.): Ophiolite genesis and evolution of the oceanic lithosphere. *Sultanate of Oman — Ministry of Petroleum and Minerals*, 771–799.

Juteau T., Berger E. & Cannat M. 1990: Serpentinized, residual mantle peridotites from the M.A.R. median valley, ODP hole 670A (21°10′ N, 45°02′ W): primary mineralogy and geothermometry. *Proc. ODP, Sci. Res.* 106(109), 27–45.

Kamenetsky V.S., Crawford A.J. & Meffre S. 2001: Factors controlling chemistry of magmatic spinel: An empirical study of associated olivine, Cr-spinel and melt inclusions from primitive rocks. *J. Petrology* 42, 655–671.

Kapsiotis A., Tsikouras B., Grammatikopoulos T., Karipi S. & Hatzipanagiotou K. 2007: On the metamorphic modification of Cr-spinel compositions from the ultrabasic rocks of the Pindos ophiolite complex (NW Greece). *Bull. Geol. Soc. Greece* 40, 2, 781–793.

Kimball K.L. 1990: Effects of hydrothermal alteration on the composition of chromian spinels. *Contr. Mineral. Petrology* 105, 337–346.

Kostopoulos D.K. 1989: Geochemistry, petrogenesis and tectonic setting of the Pindos Ophiolite, NW Greece. *Unpubl. PhD Thesis, University of Newcastle*, Newcastle, UK, 1–468.

Kubo K. 2002: Dunite formation processes in highly depleted peridotite: case study of the Iwanaidake peridotite, Hokkaido, Japan. *J. Petrology* 43, 423–448.

Mellini M., Rumori C. & Viti C. 2005: Hydrothermally reset magmatic spinels in retrogade serpentinites: Formation of "ferritchromit" rims and chlorite aureoles. *Contr. Mineral. Petrology* 149, 266–275.

Merlini A., Grieco G. & Diella V. 2009: Ferritchromite and chromian-chlorite formation in mélange-hosted Kalkan chromitite (Southern Urals, Russia). *Amer. Mineralogist* 94, 1459–1467.

Mikuš M. & Spišiak J. 2007: Chemical composition and alteration of Cr-spinels from Meliata and Penninic serpentinized peridotites (Western Carpathians and Eastern Alps). *Geol. Quart.* 51, 257–270.

Mondal S.K. & Zhou M.-F. 2010: Enrichment of PGE through interaction of evolved boninitic magmas with early formed cumulates in a gabbro-breccia zone of the Mesoarchean Nuasahi massif (eastern India). *Mineralium Depos.* 45, 69–91.

Mukherjee R., Mondal S.K., Rosing M.T. & Frei R. 2010: Compositional variations in the Mesoarchean chromitites of the Nuggihalli schist belt, Western Dharwar Craton (India): potential parental melts and implications for tectonic setting. *Contr. Mineral. Petrology* 160, 865–885.

O'Hanley D.S. & Wicks F.J. 1995: Conditions of formation of lizardite, chrysotile and antigorite, Cassiar, British Columbia. *Canad. Mineralogist* 33, 753–773.

Ohara Y. & Ishii T. 1998: Peridotites from the southern Mariana forearc: heterogeneous fluid supply in the mantle wedge. *Island Arc* 7, 541–558.

Okamura H., Arai S. & Kim Y.U. 2006: Petrology of fore-arc peridotite from the Hahajima Seamount, the Izu-Bonin arc, with special reference to chemical characteristics of chromian spinel. *Mineral. Mag.* 70, 15–26.

Proenza J.A., Gervilla F., Melgarejo J.C. & Bodinier J.L. 1999: Al- and Cr-rich chromitites from the Mayarí-Baracoa ophiolitic belt (eastern Cuba): Consequence of interaction between volatile-rich melts and peridotites in suprasubduction mantle. *Econ. Geol.* 94, 547–566.

Proenza J.A., Ortega-Gutièrrez F., Camprubì A., Tritlla J., Elìas-Herrera M. & Reyes-Salas M. 2004: Paleozoic serpentine-enclosed chromitites from Tehuitzingo, (Acatlan complex, Southern Mexico): A petrological and mineralogical study. *J. S. Amer. Earth Sci.* 16, 649–666.

Purvis A.C., Nesbitt R.W. & Hallberg J.A. 1972: The geology of part of the Carr Boyd rocks complex and its associated nickel mineralization, Western Australia. *Econ. Geol.* 67, 1093–1113.

Rassios A. & Smith A.G. 2000: Constraints on the formation and emplacement age of western Greek ophiolites (Vourinos, Pindos and Othris) inferred from deformation structures in peridotites. *Geol. Soc. Amer., Spec. Pap.* 349, 473–483.

Rassios A. & Moores E.M. 2006: Heterogeneous mantle complex, crustal processes, and obduction kinematics in a unified Pindos-Vourinos ophiolitic slab (Northern Greece). *Geol. Soc. London, Spec. Publ.* 260, 237–266.

Rassios A. & Dilek Y. 2009: Rotational deformation in the Jurassic Mesohellenic ophiolites, Greece, and its tectonic significance. *Lithos* 108, 207–223.

Reimer L. 1998: Scanning electron microscopy: Physics of image formation and microanalysis. *Opt. Sci., Springer,* Berlin, 1–515.

Rollinson H., Adetunji J., Yousif A.A. & Gismelseed A.M. 2012: New Mössbauer measurements of $Fe^{3+}/\Sigma Fe$ in chromites from the mantle section of the Oman ophiolite: evidence for oxidation of the sub-oceanic mantle. *Mineral. Mag.* 76, 579–596.

Ross J.V. & Zimmerman J. 1996: Comparison of evolution and tectonic significance of the Pindos and Vourinos ophiolite suites, northern Greece. *Tectonophys* 256, 1–15.

Sansone M., Prosser G., Rizzo G. & Tartarotti P. 2012: Spinel-peridotites of the Frido Unit ophiolites (Southern Apennine-Italy): evidence for oceanic evolution. *Period. Mineral.* 81, 35–59.

Saumur B.M. & Hattori K. 2013: Zoned Cr-spinel and ferritchromite alteration in forearc mantle serpentinites of the Rio San Juan Complex, Dominican Republic. *Mineral. Mag.* 77, 117–136.

Schwartz S., Guillot S., Reynard B., Lafay R., Debret B., Nicollet C., Lanari P. & Auzende A.L. 2013: Pressure-temperature estimates of the lizardite/antigorite transition in high pressure serpentinites. *Lithos*, http://dx.doi.org/10.1016/j.lithos.2012.11.023

Shack R.O. & Ghiorso M.S. 1991: Chromian spinels as petrogenetic indicators: thermodynamic and petrological applications. *Amer. Mineralogist* 76, 827–847.

Singh A.K. & Singh R.B. 2013: Genetic implications of Zn- and Mn-rich Cr-spinels in serpentinites of the Tidding Suture Zone, eastern Himalaya, NE India. *Geol. J.* 48, 22–38.

Spangenberg K. 1943: Die chromitlagerstätte von Tampadel in Zobten. *Z. Prakt. Geol.* 51, 13–35.

Spray J.G. & Roddick J.C. 1980: Petrology and $^{40}Ar/^{39}Ar$ geochronology of some Hellenic sub-ophiolite metamorphic rocks. *Contr. Mineral. Petrology* 72, 43–55.

Stanton R.L. 1972: Ore petrology. In: International series in the earth and planetary science. *McGraw-Hill,* New-York, 1–713.

Suita M.T.F. & Streider A.J. 1996: Cr-spinel from Brazilian mafic-ultramafic complexes: Metamorphic modifications. *Int. Geol. Rev.* 38, 245–267.

Tsujimori T., Kojima S., Takeuchi M. & Tsukada K. 2004: Origin of serpentinites in the Omi serpentinite mélange (Hida Mountains, Japan) deduced from zoned Cr-spinel. *J. Geol. Soc. Japan* 110, 591–597.

Uysal I., Kaliwoda M., Karsli O., Tarkian M., Sadiklar M.B. & Ottley C.J. 2007: Compositional variations as a result of partial melting and melt-peridotite interaction in an upper mantle section from the Ortaca area, southwestern Turkey. *Canad. Mineralogist* 45, 1471–1493.

Uysal I., Ersoy E.Y., Karsli O., Dilek Y., Sadiklar M.B., Ottley C.J., Tiepolo M. & Meisel T. 2012: Coexistence of abyssal and ultra-depleted SSZ type mantle peridotites in a Neo-Tethyan ophiolite in SW Turkey: constraints from mineral composition, whole-rock geochemistry (major-trace-REE-PGE), and Re-Os isotope systematics. *Lithos* 132–133, 50–69.

Whitechurch H. & Parrot J.F. 1978: Ecailles métamorphiques infra-peridotiques dans le Pinde septentrional (Grèce): Croûte oceanique, métamorphisme et subduction. *Cr. Acad. Sci. Paris* 286, 1491–1494.

Wylie A.G., Candela P.A. & Burkle T.M. 1987: Compositional zoning in unusual Zn-rich chromite from the Sykeville district of Maryland and its bearing on the origin of the ferritchromit. *Amer. Mineralogist* 72, 413–422.

Zhou M.-F., Sun M., Keays R.R. & Kerrich R.W. 1998: Controls on platinum-group elemental distributions of podiform chromitites: A case study of high-Cr and high-Al chromitites from Chinese orogenic belts. *Geochim. Cosmochim. Acta* 62, 677–688.

Zhou M.-F., Robinson P.T., Malpas J., Edwards S.J. & Qi L. 2005: REE and PGE geochemical constraints on the formation of dunites in the Luobusa ophiolite, Southern Tibet. *J. Petrology* 46, 615–639.